

## **Analysis of Non-linear Contact Stresses for Launched Plate Girders Bridges**

Word count (including tables and figure equivalents): 7,430

Byung-Ik Chang  
Iowa State University – CTRE  
2901 S. Loop Dr., Suite 3100  
Ames, IA 50010  
515-294-8325  
Fax 515-294-0467  
cbi@iastate.edu

### **ABSTRACT**

The incremental launching method is one of the unique methods being considered for bridge construction. Incremental launching is accomplished by assembling segments of the bridge girders behind an abutment, joining them together, and pushing the assembled segments on support bearings to their permanent position. During bridge launching there are significant forces that can develop between the launching system and the girders. For example, high contact stresses can be created in the area where the launch rollers and the lower surface of the bottom flange of a steel bridge girder come into contact. The analysis of contact-stress problems is not typically possible with closed-form solutions because of the complicated geometries, loadings, and material properties. This paper discusses the recommendations for developing a nonlinear finite-element model for analyzing the contact-stresses scenarios within the context of the Iowa River Bridge launch.

## INTRODUCTION

There are several erection methods used in bridge construction. Among these erection methods, the incremental launching method (ILM) is one unique erection method being considered for bridge construction in recent years. After over 20 years of feasibility studies, the Iowa River Bridge (IRB), crossing an environmentally sensitive river belt, was constructed by the ILM in order to minimize the impact of construction on the surrounding area. Prior to construction of the IRB on Highway 20 in north central Iowa, the launching method was used in the United States for erection of Kansas City Southern Railway bridge, near Readland, Okla. in 1970. That bridge was a steel box-girder bridge while the IRB was constructed using an steel I-girder superstructure. Past research ((1)-(8)) has studied various aspects of this unique construction method (which has been used more frequently in other countries).

During bridge launching, there are significant forces that can develop between the launching system and the girders. For example, high-contact stresses can be created in the area where the launch rollers and the lower surface of the bottom flange of a steel bridge girder come into in contact. These results from the small contact area combined with large gravity forces and could cause severe problems in the structure. Thus, the analysis of contact stress magnitudes is an important issue in designing a bridge launching system.

The analysis of contact-stress problems is not normally possible with closed-form solutions because of the complicated geometries, loadings, and material properties. Typically, problems involving complicated structural systems, including geometric and material nonlinearities, need to rely on numerical solutions, such as those from the finite element method. A review of technical literature and discussions with practicing engineers revealed that there are no useful recommendations for analyzing contact stresses for launched plate girder bridges.

## OBJECTIVE

The primary objective of this study was to develop recommendations for the analysis of contact stresses for launched plate girders that could be used by practicing engineers. For this study, finite element analyses, which were performed using the ANSYS software, were used to predict contact strains. To validate the predicted strains, comparisons were made with strains measured during the launching of the IRB.

## LITERATURE REVIEW

A literature search was conducted to collect available information on the analysis and design of ILM bridge. In the following sections, a number of pertinent articles that were reviewed are summarized. These are presented in three sections: incrementally launched bridges and finite element methods for contact problems.

### Incrementally launched bridges

After the first construction project using the ILM was completed, many articles that involved new concepts for bridge construction were published about the unique method. Literature by Per Granath, Ove Lagerqvist, and Marco Rosignoli are representative of this literature. Especially, Per Granath published several articles: Behavior of slender plate girders subjected to patch loading (1), distribution of support reaction against a steel girder on a launching shoe (2), behavior of girder webs subjected to patch loading (6), I-shaped steel girders subjected to bending moment and traveling patch loading (7), and serviceability limit state of I-shaped steel girders subjected to patch loading (8).

Granath (1) investigated the response of girders with slender webs subjected to concentrated loads using nonlinear finite element analysis. The finite element analysis results were then compared with laboratory results. A concentrated load on a plate girder occurs in various situations in engineering practice, for instance, during launching of bridge plate girders. To determine if the failure behavior depends both on the slenderness of the girder and on the loading condition, the authors tested I-shaped steel girders subjected to loading perpendicular to the flange and in the plane of the web. Granath concluded that the flange capability to resist moment in the cross section does not influence the bearing capacity of girders with slender webs for patching loading.

Marco Rosignoli (3) presented a 'reduced-transfer-matrix' concept for determine bending moment and shear forces in continuous beams for launched-girder problems. The design of a launched-steel bridge requires a considerable amount of calculations, since the highest launching stresses, such as bending moment and shear forces, have to be investigated for an extremely high number of support conditions. The purpose of his paper was to simulate, with adequate reliability, the course of launching and to obtain the highest bending moment and shear

forces. The author has also addressed this concept in his literary works entitled, “Launched Bridges” (4) and “Bridge Launching” (5), along with a general introduction to launching methods and techniques.

### **Finite element methods for contact problems**

A study was conducted by Ming Xie and D. F. Adams (9) to develop and implement a simple, but accurate, contact-modeling scheme into an existing three-dimensional, elastic-plastic, finite element analysis to study composite, short-beam specimen loaded by rigid cylinders. This scheme was found to generate results comparable to those obtained using a more rigorous contact-modeling scheme, while requiring much less computer time.

A method for contact modeling and simulation of a wheel-to-rail contact scenario was developed by Tanel Telliskivo (10). Two methods have traditionally been used to investigate the wheel-to-rail contact situation: the Hertz analytical method and simplified numerical methods based on the boundary-element method. The results of the work show that the difference in maximum, equivalent stress between traditional methods and the finite element model was small, when the minimum, contact radius was large compared to the significant dimensions of the contact area.

In a study conducted by M.G. Knight (11), the contact-stress distributions around a cylindrical (fiber) or spherical (particle) inclusion embedded in dissimilar matrices were investigated using computational techniques. The boundary-element method was shown to be versatile, accurate, and computationally inexpensive, when modeling this kind of problem, and the stress results from modeling correlated well with the present authors’ finite-element simulations. The conclusions were that the compressive stresses are higher at the interface of the fiber compared to that of the particle, and the result of including high friction coefficients is to lower the minimum, compressive stress and increase the contact angle.

## **IOWA RIVER BRIDGE LAUNCH DESCRIPTION AND DATA ANALYSIS**

Incremental launching is accomplished by pre-assembling segments of the bridge girders behind an abutment, joining them together, and pushing the assembled segments across support bearings to their permanent position. The IRB consists of two bridges: westbound and eastbound. Each of these bridges was constructed using six individual launches of approximately 91.5 m (300 ft) each. This section discusses the IRB launch and a portion of the experimental field data that were collected during the third launch of the westbound roadway. This section provides only a brief overview, however, additional information can be found in (12) and (13).

### **Bridge description**

The IRB spans 460.5 m (1,510 ft) over the Iowa River and is supported by six piers as shown in Fig. 1. The IRB consists of two parallel deck superstructures; each containing five equal spans of 92.05 m (302 ft). A 18.5-m (60.7-ft) pre-stressed concrete jump span was also constructed on each end of the steel unit. The girder webs are 3.45-m (11.33-ft) deep with the girder lines spaced at 3.6 m (11.81 ft), with a constant 22.23-mm (0.88-in.) web thickness was that designed to serve as an unstiffened bearing element for the steel dead load. In order to make the I-girder superstructure act as much as possible like a torsionally rigid box girder during launching, a very stiff system of diaphragms and lateral bracing was used. A diaphragm spacing of approximately 7.01 m (23 ft) was used for spans 2 thru 5, but was reduced to 3.51 m (11.5 ft) in the leading span that would be cantilevered during launching. All structural steel, including the girders, diaphragms, and bracing were launched with other miscellaneous bracing to minimize the transport of materials following the launch.

### **Launching system description**

To facilitate launching, steel rollers, 457.2 mm (18 in.) in diameter and 152.4 mm (6 in.) wide, were used to reduce longitudinal resistance. A 44.65-m (146.5-ft) long, tapered-steel-nose assembly was attached to the beginning of the structure, and consisted of two girders that were in line with the two interior girders of the bridge. This tapered nose section was used to lift the permanent girders upward over each pier and to reduce the negative bending moment generated during launching. A 7.32-m (24-ft) long, framed-steel-tail assembly was temporarily attached to the end of the girder launching system. This launching tail distributed the hydraulic-jacking force to the girders.

Figure 1 illustrates an elevation view for an interior girder at a single point during Launch 3 of the westbound bridge. At locations where the girder bottom flange changed thickness, tapered ramps were used to

allow a girder to be smoothly pushed over the rollers at each support. For instance, at the end of the field splice that is the closest to the nose assembly, an upward tapered ramp (Up ramp) was used while a downward tapered ramp (Down ramp) was used at the other end of a field splice. The “up” and “down” ramps are essentially wedge-shaped steel plates. The field splices, up ramps, and down ramps are notated as FS1 through FS13, UR1 and UR2, and DR1 and DR2 respectively in Fig. 1. To support the girders within the launch pit, four temporary rollers, denoted as RA, RB, RC, and RD, were installed behind Pier 6.

### Experimental data collection

Contact-strain data were collected during Launch 3 of the westbound roadway for the IRB. To accomplish this, strain gages were installed on two girders, Girder C (an interior girder) and Girder D (an exterior girder), on the lower portions of the girders, as shown in Fig. 2. This instrumentation was installed at the cross section labeled “Instrumented location” in Fig. 1 (shown at the point of highest contact stress where it passes over Pier 6). Girder C has web-plate dimensions of 3451.23 mm (135 7/8 in.) by 22.23 mm (7/8 in.), top flange-plate dimensions of 374.65 mm (14 3/4 in.) by 22.23 mm (7/8 in.), and bottom flange-plate dimensions of 498.48 mm (19 5/8 in.) by 31.75 mm (1 1/4 in.). Girder D has the same dimensions as those for Girder C with the exception that the thickness of the bottom flange-plate which is 28.58 mm (1 1/8 in.). The gages on the bottom flange were oriented in the longitudinal direction of the girders, and the gages on the web were oriented in the vertical direction. As shown in Fig. 2, a total of thirteen strain gages were mounted on each girder.

The gage notation shown in Fig. 2 relates each gage to a specific location on the cross-section and will be referred to in subsequent sections. Specially, **DS** represents Girder **D** and Southern side, **BW** represents **B**ottom gages on the **W**eb, and **OBF** represents **O**uter gages on the **B**ottom **F**lange. For example, **DSTW** indicates Girder **D**, Southern side, Top gages, and on the **W**eb-plate, **CBF** indicates Girder **C** and on the center of the lower surface of **B**ottom **F**lange, and **CSOF** indicates Girder **C**, Southern side, **O**uter gage and on the upper surface of the bottom **F**lange. The strain data were recorded every 0.25 second after the gage readings were initially zeroed. As a result, the gage readings represent changes in the total strain from the strain at the initial position.

### IRB CONTACT MODELING APPROACH AND RESULTS

Nonlinear structural behavior occurs from contact nonlinearities, geometric nonlinearities, and/or material nonlinearities. For the IRB, the girder flange was in-and-out of contact with the roller surface and some of the measured strains during launching exceeded the material yield strain. These behaviors require that both contact and material nonlinearities be considered for the contact-stress analysis of the IRB.

Prior to attempting to model a complete launched girder, a Hertz contact problem was analyzed as a preliminary investigation. For the Hertz contact problem, a finite element model was generated with a 1.27 mm (0.05 in.) mapped mesh in the contact area. The contact-stress results from the finite-element modeling were compared with the results obtained from a closed-form solution. Based on the contact stress from the finite-element modeling and the traditional method, the finite-element modeling was found to produce accurate results.

To complete all analyses the following assumptions were made: loads were statically applied, diaphragms provided no lateral-load distribution, girders had a constant cross section (for global analysis only), loads included only the girder self-weight, and girders were centered on the launching rollers.

### Introduction of nonlinear analysis in ANSYS

The commercial Finite Element Analysis software ANSYS 6.1 (14) was used to perform the nonlinear analysis discussed herein. The following discussion was written using specific terminology for ANSYS. However, the concepts and applications are widely applicable.

To solve contact and material nonlinear problems, ANSYS uses an incremental solution procedure, the Newton-Raphson equilibrium-iteration, to achieve convergence of displacement to a specified tolerance of 0.1%. In each iteration procedure, the total external load within a load step is applied in increments over a certain number of sub-steps. The solution results are then saved in a results file, which can be conveniently reviewed in the general postprocessor.

### **IRB Model geometry and material properties**

Since the IRB contact model was symmetric in transverse geometry, transverse load conditions, and expected deformation of the structure, only one half of the girder and the roller were modeled, as shown in Fig. 3. To create the model, individual volumes (flanges, web, and fillets) were created and then connected to each other. The contact-pair concept was then applied to model the contact geometry between the surface of the roller and the lower surface of the bottom flange.

The material properties for the selected element are those of steel: density of 7849 kg/m<sup>3</sup> (490 lb/ft<sup>3</sup>) applied by means of a gravity factor, a modulus of elasticity of 200 GPa (29,000 ksi), and a Poisson's ratio of 0.3. A friction coefficient of 0.3 for the contact analysis was also specified.

### **Modeling considerations of the IRB contact analysis**

For a three-dimensional solid structural analysis, several modeling decisions must be made to obtain accurate stress-strain information while at the same time minimizing the data-processing time. Element type and mesh generation, which includes mesh density and mesh style, are some of the early considerations. For contact and material nonlinearities, contact elements and the plasticity options must also be properly selected.

For the analysis of beam type structures such as IRB, the girder-aspect ratio (girder length vs. depth) considered in the analysis is also an important consideration. In order to minimize the data-processing time and the number of elements in the finite element model, the most suitable girder-aspect ratio must be determined. Also the boundary condition approach can be a specific modeling consideration.

In the IRB contact modeling, the boundary conditions, which are the bending moments, shear forces, rotations, and deflections from a classical-beam analysis, were applied to the three-dimensional model. To simplify the technique to represent the internal bending moment, loads were applied in the longitudinal direction at the upper most nodes of the top flange and at the lower most nodes of the bottom flange of the member cross section. To account for the vertical shear force at the boundaries of this model, equally distributed loads were applied in the vertical direction at the nodes of the elements along the mid-thickness of the web plate. If only a portion of the model requires a finer mesh such as in contact area, sub-modeling could be one possible technique for obtaining more accurate results.

#### *Element type*

There are several possible types of structural three-dimensional-solid elements that may be used in ANSYS for this type of analysis. The SOLID45, 72, 73, 92, and 95 elements are possible elements types. The descriptions for these elements are given in Table 1. Table 1 contains the information needed to identify similar element types in other FEM packages.

Of the five element types that are available and were previously mentioned, the SOLID45 element has the fewest degrees of freedom. As such, the SOLID45 element was considered as the baseline. The other types of elements were investigated and the strain results were then compared with those that were obtained when SOLID45 elements were used. In short, given the relative accuracy and data processing time, the SOLID45 element was selected as the most appropriate element type for this type of analysis. As an example, the predicted, vertical strains in the web plate that are associated with the different types of elements along with the measured strains on the north and south force of the web plate are shown in Fig. 4 (a). The strain distribution across the height of the web plate was similar for all five element types.

Contact-analysis problems generally require a smaller element size near the contact region than for regions that are located away from the contact region. However, smaller element sizes increase the number of elements and data-processing time. For the IRB, a 12.7 mm (0.5 in.) mesh size was used around the contact area while a coarser mesh was used in the other regions. Unfortunately, computer limitations dictated that a smaller mesh size could not be used. It is the authors' opinion that a smaller mesh is needed to analyze the stresses in the close vicinity to the roller. Since the roller and flange plate have a surface-to-surface contact relationship, TARGE170 and CONTA174 elements were used to define the contact pair. For analysis of the IRB contact analysis, the middle 1 ft (0.305 m) of the lower surface of the bottom flange, was specified as a contact surface and half of the roller surface was specified as the target surface.

### *Mesh generation*

Figure 4 (b) shows the predicted, vertical, strain distribution along the height of the web plate when a free mesh and a mapped mesh is used to model the portion of the girder near the support roller. These analyses were performed using the SOLID45 elements, a girder-aspect ratio of four, and the member-end, force-based approach discussed above. The two mesh styles produced similar strain patterns to that obtained from the field data, but the free-mesh model required more elements and approximately 70% more data-processing time. Thus, even though a mapped mesh takes a longer time to generate, a mapped mesh is the most suitable mesh style for this analysis in light of the significant processing time.

### *Contact and Material nonlinearity*

A “large” number of contact regions should be assumed for both the contact and target surfaces to ensure that the contact behavior is correctly modeled. This results from the fact that the size of the contact regions are generally unknown until after the analysis has been completed. ANSYS supports a “contact-pair” concept, which can reduce the time required to create the contact elements and to select the contact and target surfaces.

Nonlinear, stress-strain relationships are a common form of nonlinear structural behavior. Many factors can influence a material’s stress-strain properties, including load, environmental conditions, and the amount of time that a load is applied. To model the stress-strain behavior for the IRB materials, the Multilinear Isotropic Hardening option (MISO tables in ANSYS) was required. The MISO table uses the von Mises yield criteria, coupled with an isotropic, work-hardening assumption.

### *Girder aspect ratio*

Elementary-beam theory assumes that the length of a span is significantly larger than the depth of the section. To use the member-end forces and deformations from the classical-beam analysis, the girder-aspect ratio used in a model of only a portion of a beam must also satisfy the assumptions of elementary-beam theory. Therefore, defining the minimum effective girder-aspect ratio is very important. To evaluate this, different aspect ratios were investigated to determine the minimum effective girder aspect ratio needed to apply the classical-beam analysis results to a three-dimensional model.

Too small of an aspect ratio will produce inaccurate results and too large of an aspect ratio will significantly increase the number of elements and data-processing time. To determine the best girder-aspect ratio, three-dimensional solid analyses were performed with ratios of 2, 4, and 6. The predicted strain results from the analyses for these aspect ratios were compared to the measured strains that were obtained during the field testing. Figure 5 (a) illustrates the strains for Girder C at the launch distance of 251.17 m (823.5 ft). The analysis using a ratio of six required 30 % more data-processing than that using an aspect ratio of four. Thus, as there was minimal difference in the analysis accuracy when using an aspect ratio of four and six, an aspect ratio of four was selected as the girder-aspect ratio to be used for this analysis.

### *Load or displacement boundary conditions*

Two different sets of boundary conditions can be used for the three-dimensional finite-element modeling. One set of boundary conditions involves using the member-end forces (shear forces and bending moments) that were computed from a classical beam analysis. The other set of boundary conditions involves the member-end displacements (rotations and deflections) from the same classical-beam analysis.

The web strains that were predicted by the member-end force based approaches (shown in Fig. 5(b)) are in close agreement with the measured strains in the web plate. Additionally, less processing time was required for this approach than that needed by the member-end displacement approach. Therefore, the member-end, force-based approach was selected as the most effective method for analyzing the structure.

### *Sub-modeling*

To increase the accuracy of the results in a specific region, a sub-modeling technique is commonly considered. Sub-modeling (15) is also known as the cut-boundary displacement method or the specified-boundary displacement method. With this technique, nodal displacements calculated on the cut boundary of a coarse model are interpolated as boundary conditions for a sub-model.

Sub-modeling is based on St. Venant's principle which states that if an actual distribution of forces is replaced by a statically equivalent system, the distribution of stress and strain is altered only near the regions of load application. This implies that stress-concentration effects are localized; therefore, if the boundaries of the sub-model are far enough away from a stress concentration, reasonably accurate results can be calculated in the sub-model.

An area with a width of 0.305 m (1 ft) and a height of 0.305 m (1 ft) was sub-modeled with a mesh size of 6.35 mm (0.25 in.) (due to the limited computer hardware resources, an analysis with a mesh size smaller than 6.35 mm (0.25 in.) could not be conducted because the refined mesh caused much larger computer processing time to analyze the model). Improved results for the vertical strains in the web plate were not obtained using sub-modeling with the 6.35 mm (0.25 in.) mesh size. However, it is believed that sub-modeling with even smaller elements could improve the stress predictions in the close vicinity to the roller.

## Results

Based on the modeling features investigated and discussed above, a final model for Girder C, an interior girder, was developed with a mapped mesh using SOILD45 element with a 12.7 mm (0.5 in.) element size and a girder-aspect ratio equal to four. The analysis was performed using the member-end, force-based approach. Similarly, a model for Girder D, an exterior girder, was also developed using the same approach.

Figure 6 shows the vertical strains in the lower portion of web plate for both Girders C and D, respectively, when the instrumented section was near Pier 6. Generally, the predicted strains followed a similar pattern to the pattern that was obtained from the field data, but the predicted strain at some of the launch stages differed by between 20% and 60% from the measured strains (DSBW and DNBW). These strain differences were especially true for Girder D. Large differences between the predicted and measured strains like these could occur if the rollers were not centered about the mid-thickness of the web plate, if a girder was not fully resting on a roller, or if other behaviors were present not in agreement with the previously mentioned assumptions.

Figure 7 shows the longitudinal strains in the upper surface of the bottom-flange plate for Girders C and D, respectively, near Pier 6. In general, the predicted, longitudinal strain along the width of the upper surface of the bottom-flange plate significantly deviated from and did not follow a strain pattern similar to that obtained from the field data. These strain differences were especially true at the locations that were within the width of the roller. These differences between the predicted and measured strains could be because the measured strains might be influenced by the diaphragms between bridge girders and because the girders were probably not centered over the support rollers. Additionally, the bottom flange mesh size was probably not small enough to obtain accurate results in this region.

The longitudinal strains on the lower surface of the bottom flange of Girders C and D near Pier 6 are shown in Fig. 8. No center gage data (i.e., location CBF and DBF) were obtained beyond the 251.2-m (823.5-ft) launch stage because these gages were destroyed when they came in contact with a roller. Before the 251.2-m (823.5-ft) launch stage, the measured, center, gage-strain values (CBF and DBF) for the bottom flange dramatically increased up to 4390 micro-strains and 7634 micro-strains (both in compression) for Girder C and D, respectively. Except for the center gage strains for both Girders C and D, the strains which were predicted by the ANSYS model typically followed a similar pattern to that for the measured strains. One possible reason for the significant difference between the predicted strains and the measured strains for the center gages could be because the 12.7 mm (0.5 in.) element size was not small enough at the contact region. Due to the limited computer hardware resources, an analysis with a mesh size smaller than 12.7 mm (0.5 in.) could not be conducted because the finer mesh size exceeded the available computer resources.

## CONCLUSIONS

In general, the vertical strains in the web plates for Girder C and D that were predicted by the finite element analyses had patterns and magnitudes similar to those measured in the field. However, the predicted longitudinal strains in the bottom-flange plate for both girders in the contact region were significantly different from those measured strains. These differences are likely due to the assumptions made during the analyses and computer resource limitations that prevented using very small element size in the contact region. The following conclusions are based on the finite-element studies.

- The best approach for modeling contact stress problems is to analyze the entire structure. However, simplification of the model is generally required due to a variety of unknown and unpredictable geometric abnormalities and limited hardware resources.

- A girder-aspect ratio of four or more is needed. Depending on how the internal loads are simulated, an aspect ratio of 8 or more may be needed.
- The member end force-based approach for modeling the boundary conditions for a three-dimensional model provides better strain results than those that were obtained using the member end displacement-based approach.
- A mapped mesh required less data processing time than a free mesh. The recommended mesh style even though it requires more time to generate than that for a free mesh.
- A tetrahedral-solid, shape elements, such as the SOLID72 and SOLID92 elements that were oriented using a free mesh, exhibited similar results for the vertical strains in the web plate but require more data-processing time and a larger number of elements than hexahedron-solid elements, such as the SOLID45, SOLID73, and SOLID95 elements that were oriented using a mapped mesh.
- Elements that have additional degrees of freedom, such as the SOLID73 and SOLID72 elements, and a higher-order element, such as the SOLID95 element require more data-processing time, more elements, and produced similar results to lower order elements for the vertical strains in the web plate when compared with the lower-order elements.
- Mesh size near the contact region must be smaller than 12.7 mm (0.5 in.). Based on work not presented here, the element size may need to approach 1.27 mm (0.05 in.) to give high accuracy results.
- Sub-modeling with a 6.35 mm (0.25 in.) element size did not provide increased accuracy for the predicted, longitudinal strains in the bottom flange for Girder C, when compared to those strains that were predicted by the full finite-element model.

## ACKNOWLEDGMENTS

The author would like to acknowledge the Iowa Department of Transportation for sponsoring the IRB project.

## REFERENCES

1. Granath, Per. Behavior of slender plate girders subjected to patch loading. *Journal of Constructional Steel Research*, Vol. 42, No. 1, 1997, pp. 1-19.
2. Granath, Per. Distribution of support reaction against a steel girder on a launching shoe. *Journal of Constructional Steel Research*, Vol. 47, No. 3, 1998, pp. 245-270.
3. Rosignoli, Marco. Solution of the continuous beam in launched bridges. *Proceedings of the Institution Civil Engineers. Structures and buildings*, Vol. 122, No. 4, 1998, pp. 390-398.

4. Rosignoli, Marco. Launched Bridges; Prestressed Concrete Bridges Built on the Ground and Launched into Their Final Position. ASCE, Virginia, 1998.
5. Rosignoli, Marco. Bridge Launching. Thomas Telford Ltd, Parma, Italy, 2002.
6. Granath, Per. Behavior of girder web subjected to patch loading. *Journal of Constructional Steel Research*, Vol. 50, No. 1, 1999, pp. 49-69.
7. Granath, Per. I-shaped steel girders subjected to bending moment and traveling patch loading. *Journal of Constructional Steel Research*, Vol. 54, No. 3, 2000, pp. 409-421.
8. Granath, Per. Serviceability limit state of I-shaped steel girders subjected to patch loading. *Journal of Constructional Steel Research*, Vol. 54, No. 3, 2000, pp. 387-408.
9. Xie, Ming.; Adams, D. F. "Contact Finite Element Modeling of the Short Beam Shear Test for Composite Materials" *Computers & Structures*, Vol. 57, No. 2, pp. 183-191, 1995.
10. Telliskivi, Tanel. A tool and a method for FE analysis of wheel and rail interaction. Royal Institute of Technology; Department of Machine Design. 2002.
11. Knight, M.G. "Parametric study of the contact stresses around spherical and cylindrical inclusions." *Computational Material Science*, Vol. 25, pp. 115-121, 2002.
12. Iowa Department of Transportation. The US20 Iowa River Bridge: Providing for the Future, Preserving Iowa's Past. 2000. [www.iowariverbridge.org](http://www.iowariverbridge.org). Accessed July 31, 2004.
13. Wipf, Terry J. et al. US 20 Iowa River Bridge: Launched Girder Bridge Monitoring. Ames, IA: Iowa State University; Bridge Engineering Center, 2004.
14. Swanson Analysis System, Inc. ANSYS User's Manual for Revision 5.0 Procedures. Huston, PA, 1992.
15. Imaoka, Sheldon. Sheldon's ANSYS tips and tricks: Nonlinear sub-modeling. <http://ansys.net/ansys/?mycat=search&mytype=All&mysort=alpha&mystring=submodeling>. Accessed July 31, 2004.

**LIST OF TABLES**

TABLE 1 Three-dimensional solid element in ANSYS

**LIST OF FIGURES**

FIGURE 1 IRB launch 3 for the westbound roadway

FIGURE 2 Girder cross sections and strain-gage identifications for Launch 3

FIGURE 3 IRB model geometry

FIGURE 4 Model comparison for Girder C at stage 823.5-ft using different types of element and mesh styles

FIGURE 5 Model comparison for Girder C at stage 823.5-ft using different aspect ratio and boundary condition

FIGURE 6 Vertical strains in the lower part of the web plate from the 823.0-ft to 824.0-ft launch stages

FIGURE 7 Longitudinal strains in upper surface of bottom-flange plate from the 823.0-ft to 824.0-ft launch stages

FIGURE 8 Longitudinal strains in lower surface of bottom-flange plate from the 823.0-ft to 824.0-ft launch stages

TABLE 1 Three-dimensional solid element in ANSYS

Type of element	Number of nodes	Degrees of freedom	Title
SOLID45	8-nodes	UX, UY, UZ	Structural solid
SOLID72	4-nodes	UX, UY, UZ, ROTX, ROTY, ROTZ	Solid with rotations
SOLID73	8-nodes	UX, UY, UZ, ROTX, ROTY, ROTZ	Solid with rotations
SOLID92	10-nodes	UX, UY, UZ	Tetrahedral solid
SOLID95	20-nodes	UX, UY, UZ	Structural solid

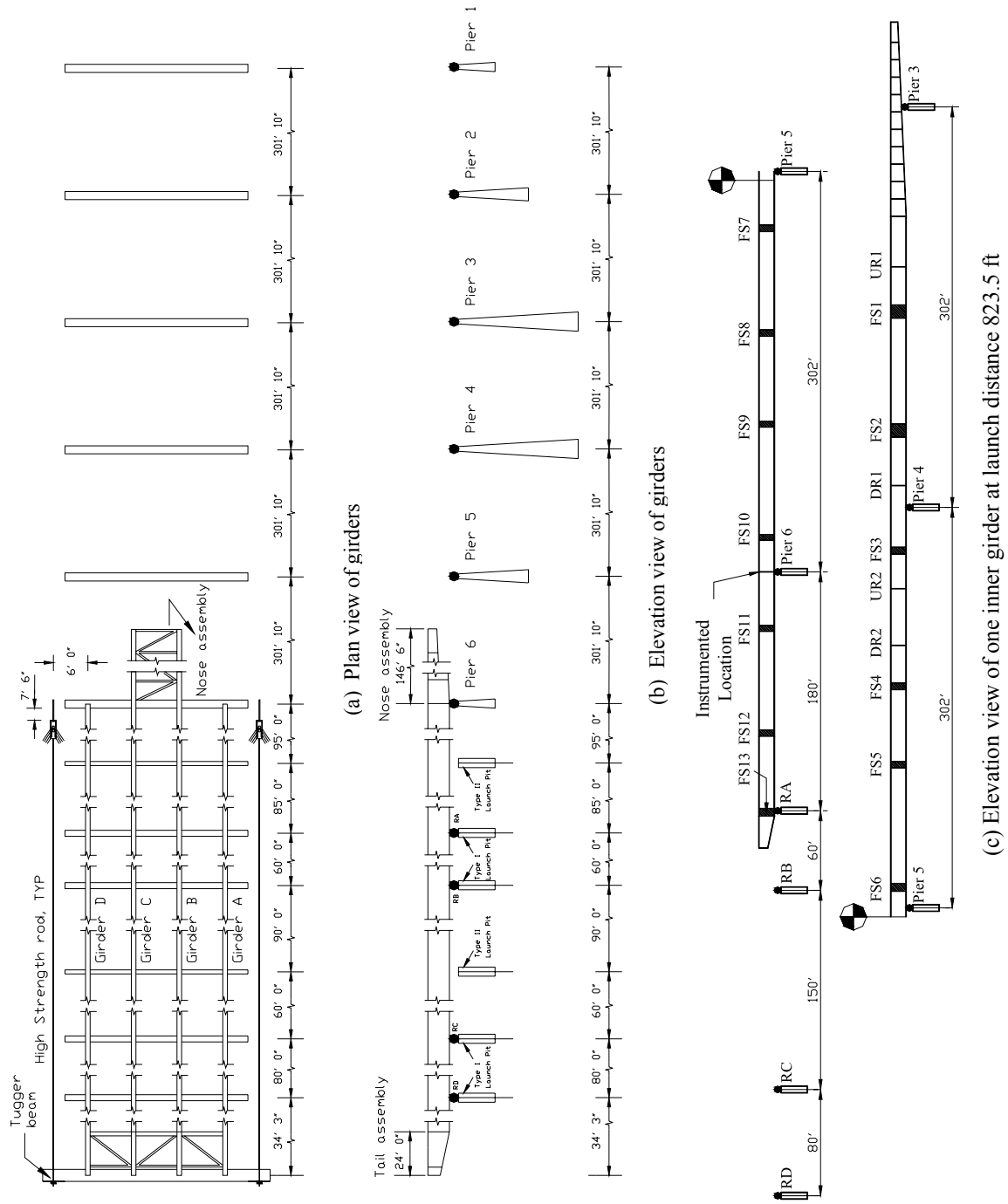
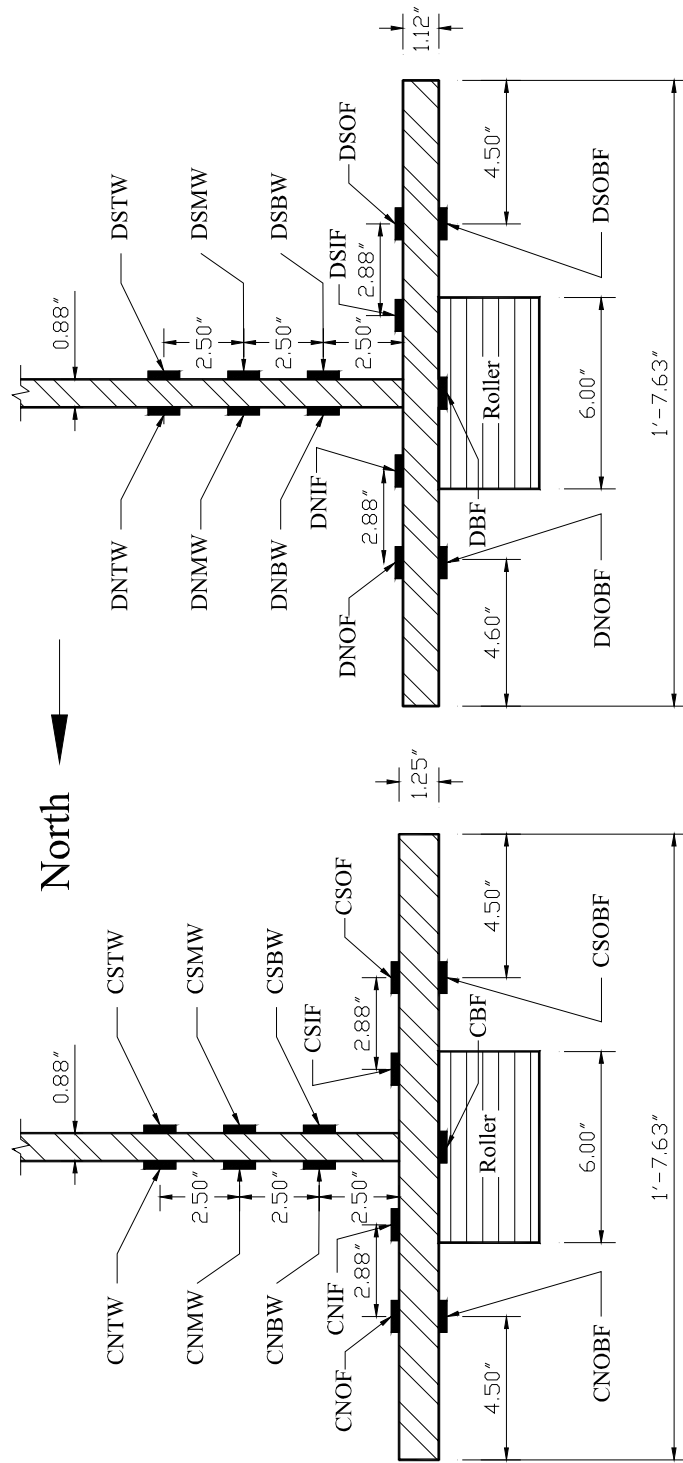


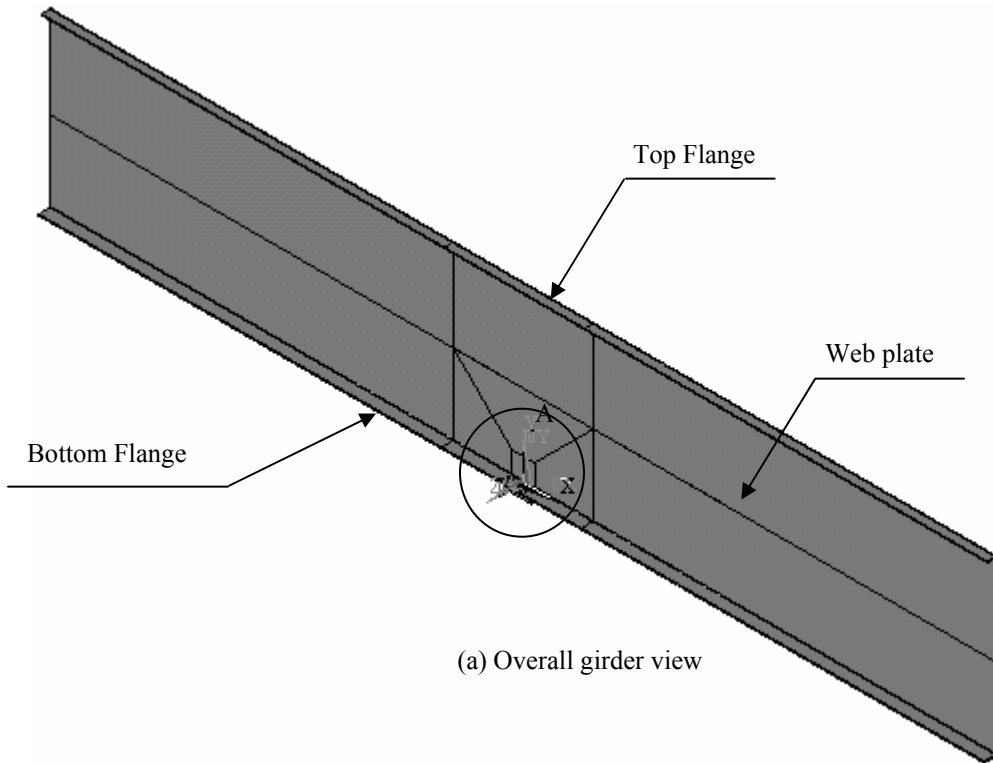
FIGURE 1 IRB launch 3 for the westbound roadway



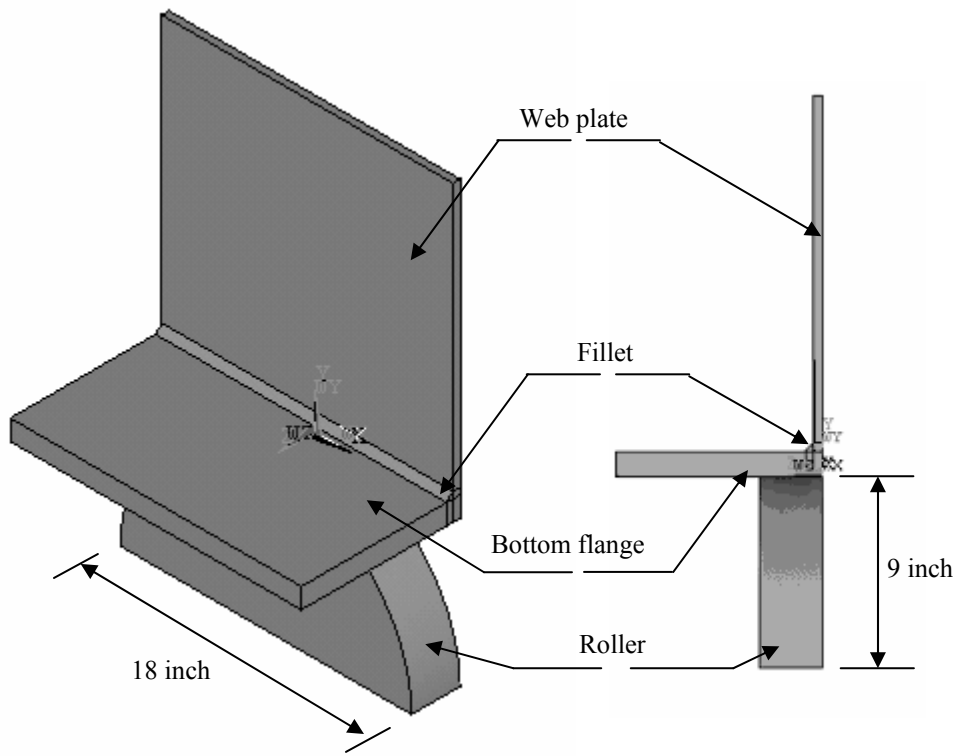
(b) Girder D

(a) Girder C

FIGURE 2 Girder cross sections and strain-gage identifications for Launch 3



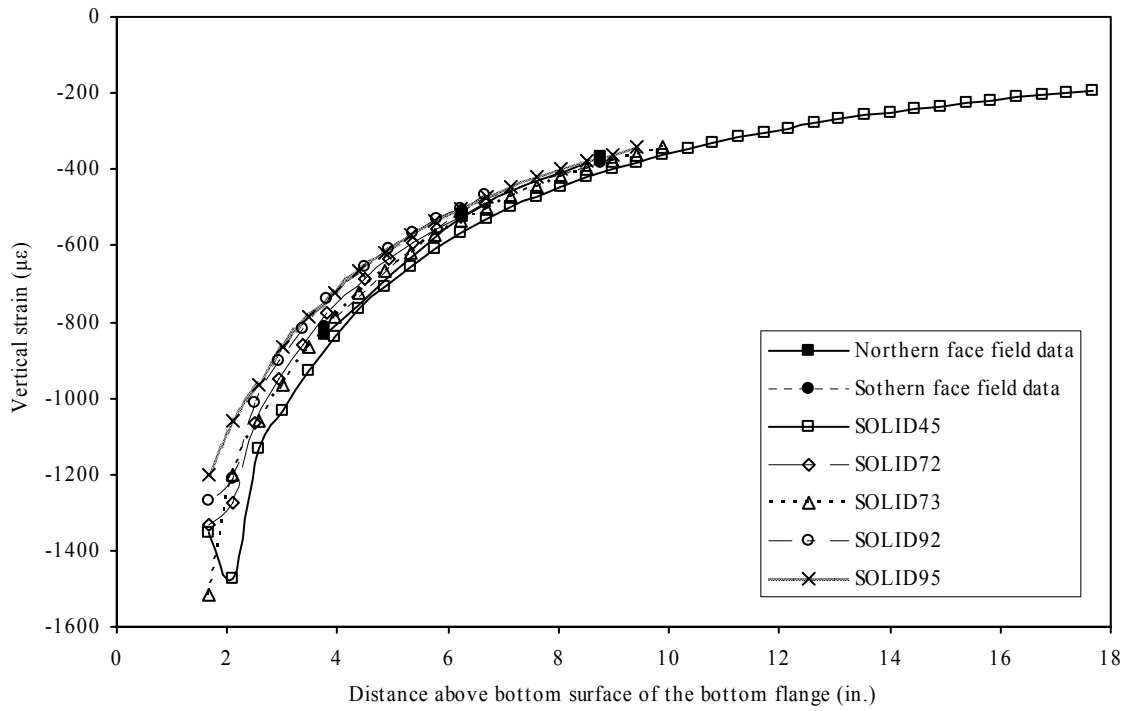
(a) Overall girder view



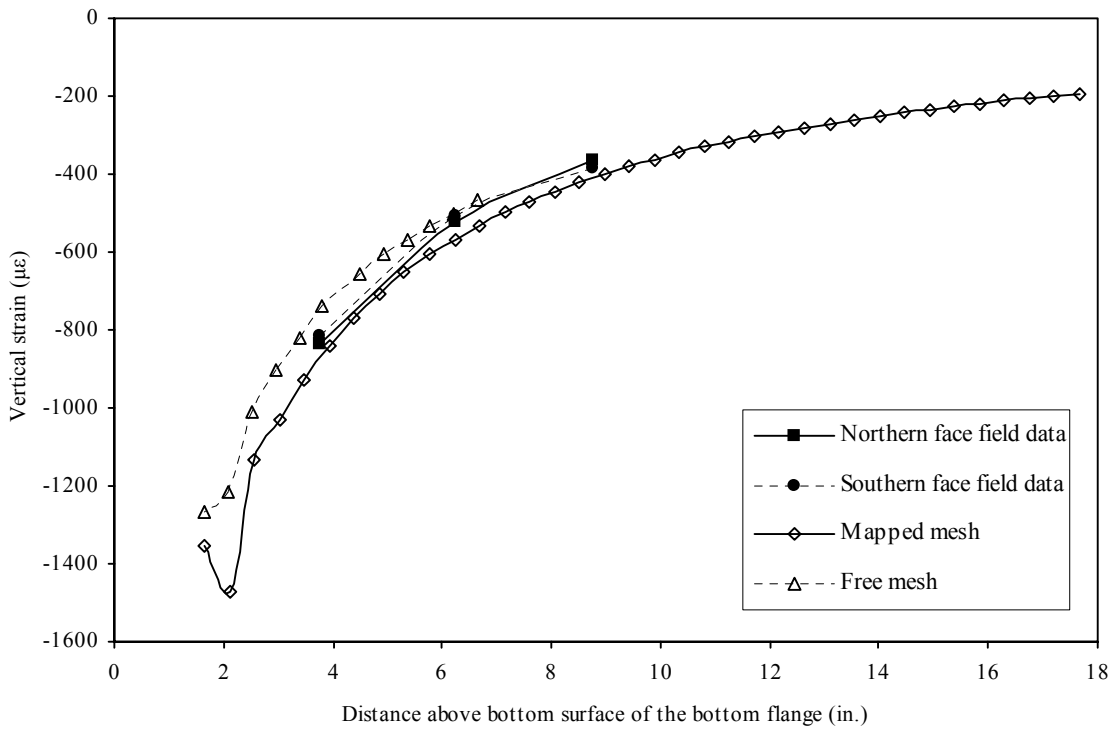
(b) Detail of overall girder; A

(c) Side view of detail shown in (b)

FIGURE 3 IRB model geometry

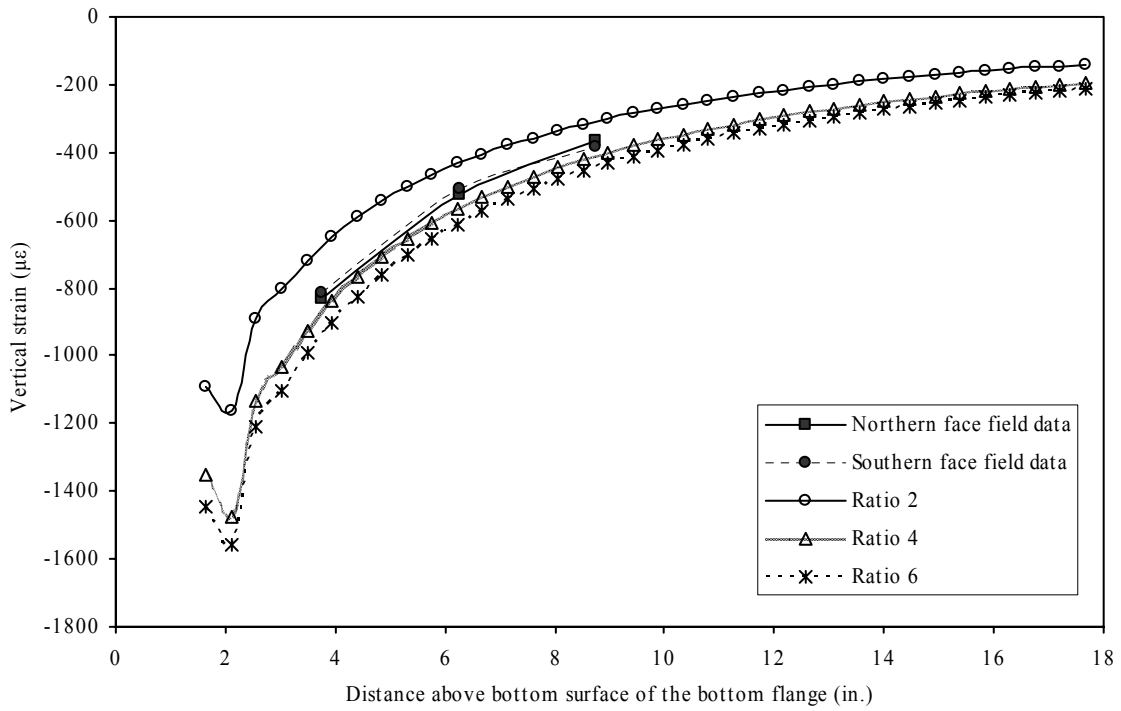


(a) Types of element

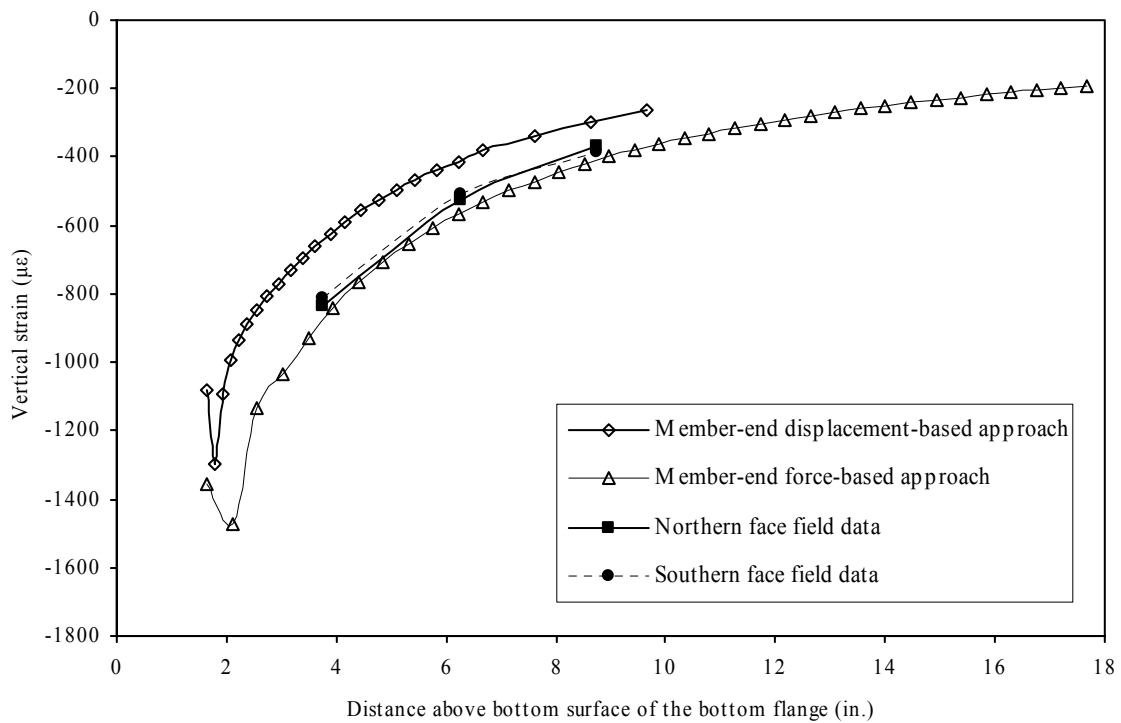


(b) Free and mapped meshes

FIGURE 4 Model comparison for Girder C at stage 823.5-ft using different types of element and mesh styles

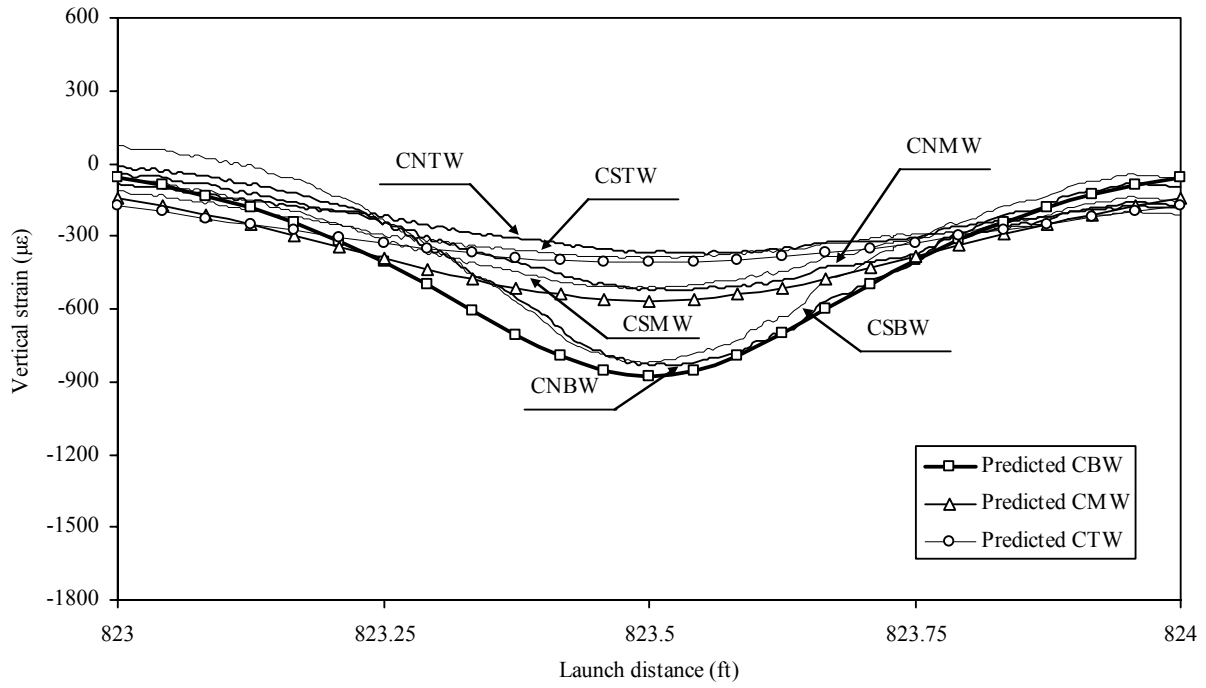


(a) The girder-aspect ratios

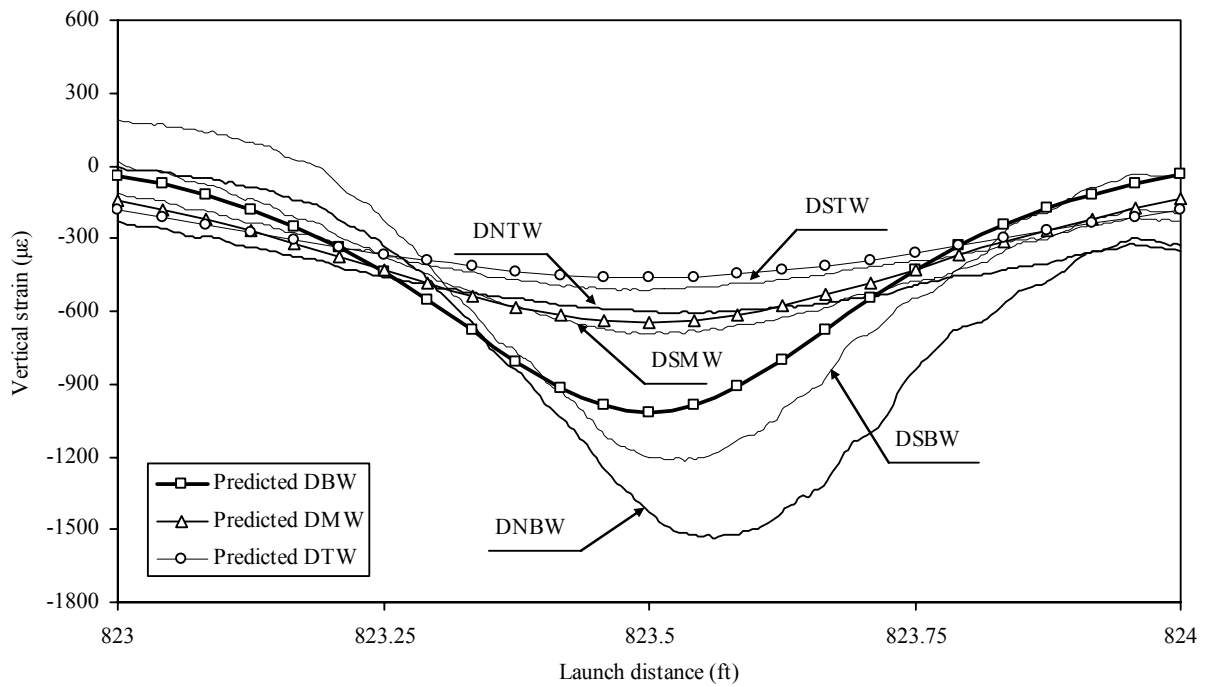


(b) The load and displacement boundary

FIGURE 5 Model comparison for Girder C at stage 823.5-ft using different aspect ratios and boundary conditions

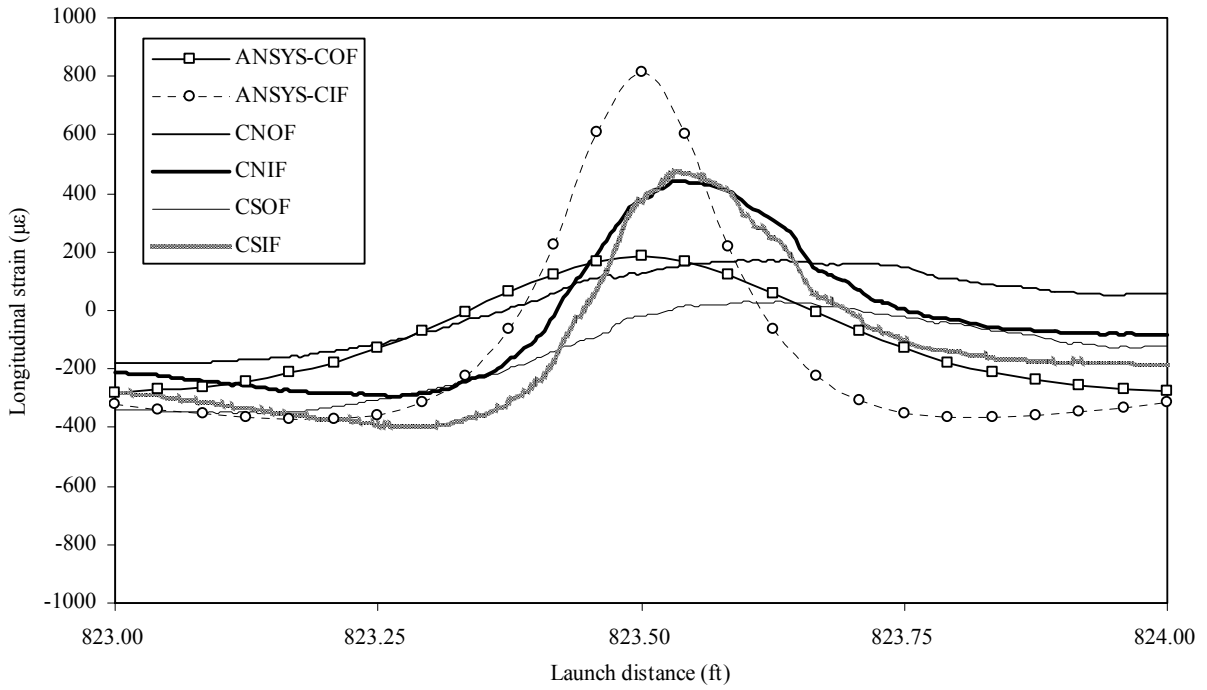


(a) Girder C

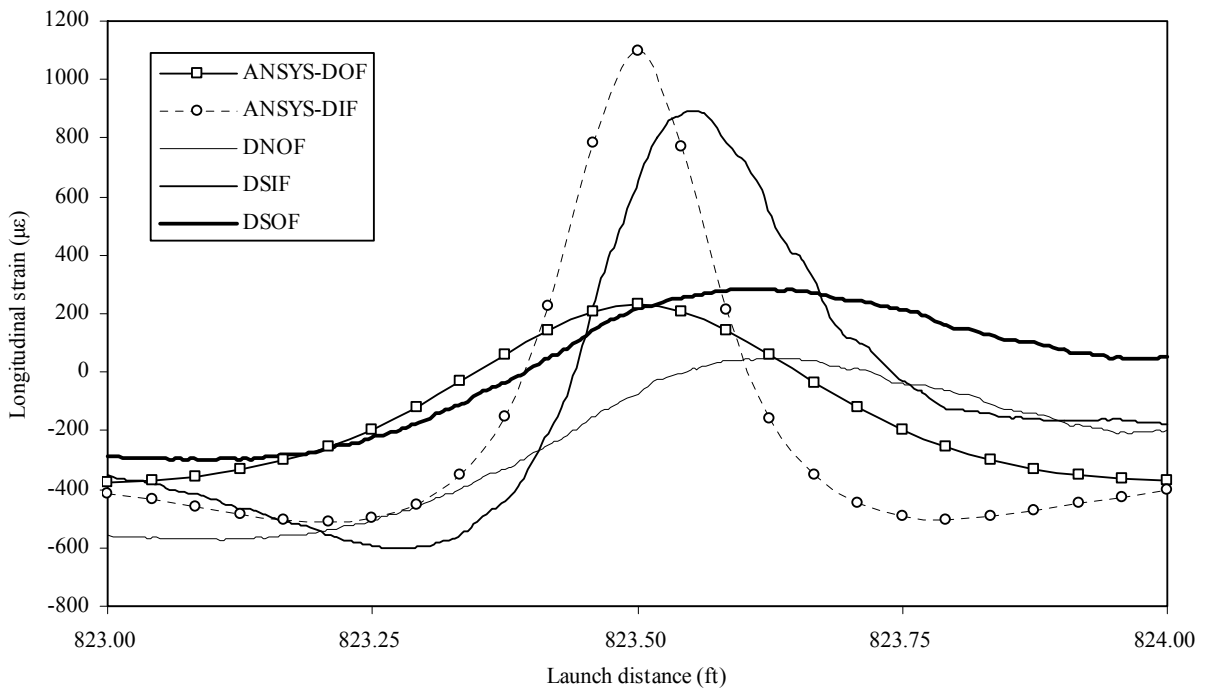


(b) Girder D

FIGURE 6 Vertical strains in the lower part of the web plate from the 823.0-ft to 824.0-ft launch stages

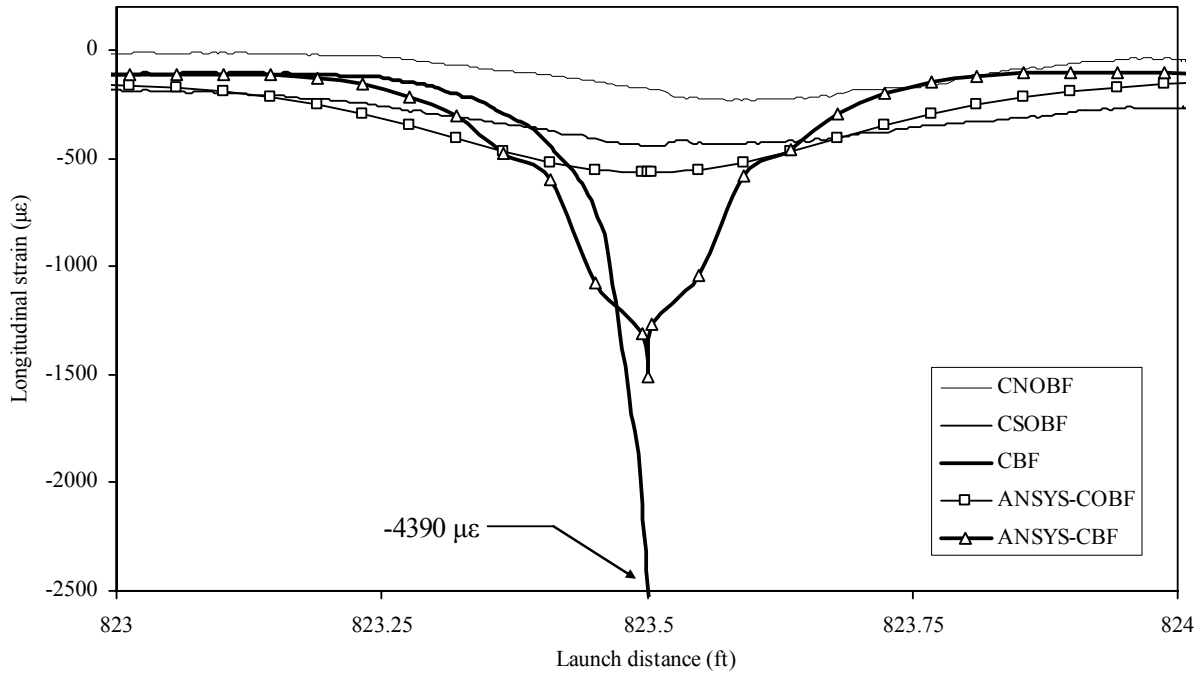


(a) Girder C

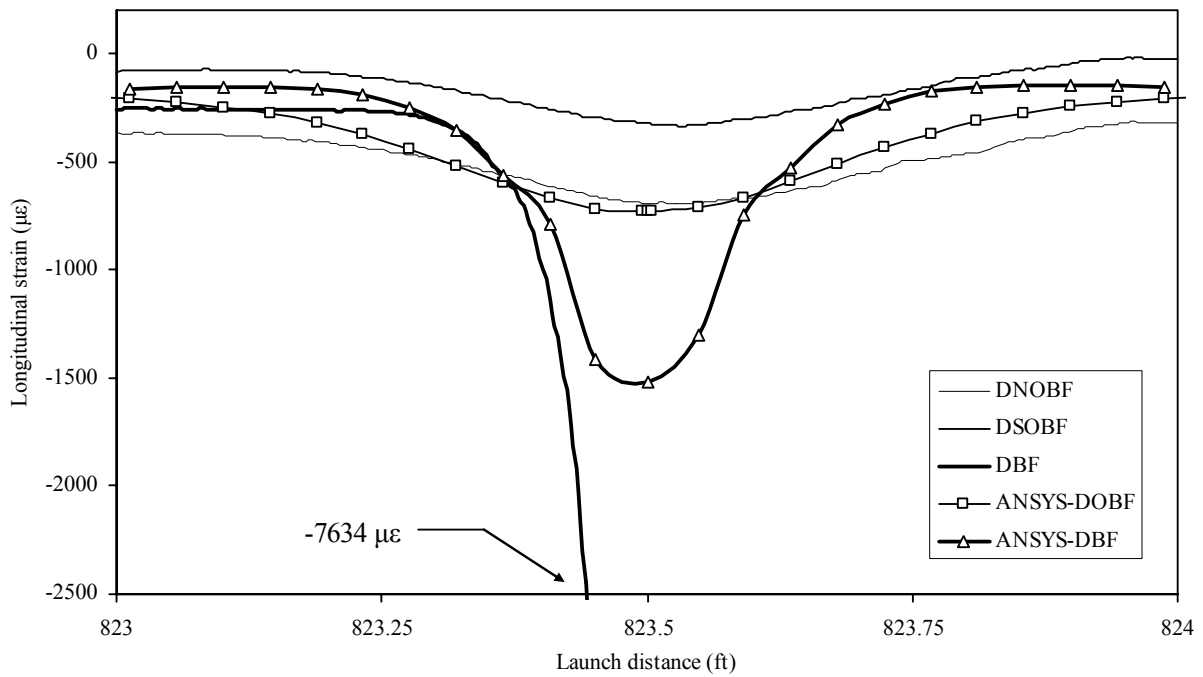


(b) Girder D

FIGURE 7 Longitudinal strains in upper surface of bottom-flange plate from the 823.0-ft to 824.0-ft launch stages



(a) Girder C



(b) Girder D

FIGURE 8 Longitudinal strains in lower surface of bottom-flange plate from the 823.0-ft to 824.0-ft launch stages